Label-Free DNA Detection on Nanostructured Ag Surfaces

Hsin-I Peng,[†] Christopher M. Strohsahl,[‡] Kathryn E. Leach,[§] Todd D. Krauss,[§,⊥] and Benjamin L. Miller[†,¶,*]

[†]Department of Biomedical Engineering, University of Rochester, Rochester, New York 14627, [‡]Lighthouse Biosciences, Rochester, New York 14586, [§]Department of Chemistry, University of Rochester, Rochester, New York 14627, [⊥]The Institute of Optics, University of Rochester, Rochester, New York 14627, and [¶]Department of Dermatology and the Center for Future Health, University of Rochester, Rochester, New York 14627

ARTICLE

ABSTRACT The dramatic local electric-field enhancement property of Ag nanoparticles was used as the basis to significantly increase the signal output of a novel label-free (or "self-labeled") fluorescence-based DNA detection system. In response to identical amounts of analyte, nanostructured Ag substrates provided a posthybridization fluorescent sensor response over 10-fold larger than the response from planar Au substrates. Detection performance strongly depended upon the Ag substrate roughness. Consistent with work by others on metal-enhanced fluorescence, fluorescence intensity also depended strongly on the distance between the fluorophore and the Ag substrate surface. Adjusting the surface roughness, amount of the Ag deposited on the surface, and the DNA probe length allowed for production of an optimized response. In addition to constituting a novel label-free DNA sensor, we anticipate that these structures will provide a unique platform for testing concepts in plasmonics.

KEYWORDS: Ag nanoparticles · DNA detection · DNA hairpins · metal enhanced fluorescence

Array-based DNA sensors have become nearly ubiquitous over the past decade, in tandem with the unraveling of the genetic code of many living organisms.[1,2] Such sensors have shown great promise in medical diagnosis, biowarfare agent detection, and forensic analysis.[3,4] Currently, much of the research in this area is focused on the development of "label-free" or "self-labeled" DNA detection systems, where detection readouts can be measured directly from the analyte without additional target manipulation. These methods include, but are not limited to, optical sensors employing molecular beacons,[5−10] electrical,[11−14] surface plasmon-based,[15,16] and microgravimetric DNA detection systems.[17,18]

Nanotechnology has recently opened a new horizon for DNA detection. This is manifested in the development of novel nanoenabled detection schemes including colorimetric,[19,20] scanometric,[21] and microarray-based detection systems incorporating metallic nanostructures.[22] It is well established that metallic nanoparticles (NPs) are able to dramatically increase molecular fluorescence intensities, the result of an enhanced local electric field surrounding the metallic NPs that is induced by the incident light.[23,24] The level of electromagnetic enhancement is a strong function of physical parameters such as NP size, shape, and coincidence between the NP resonance wavelength and the dye absorption/emission wavelength.[25−27] This strong local electric field concomitantly causes a decrease in the excited state lifetime (i.e., increasing the fluorescence decay rate) and an increase in the photostability of the fluorophore.[28−30] On the other hand, fluorescence amplification is not universally observed near the surface of metallic NPs: quenching results when the fluorophore is placed in very close proximity (<5 nm) to the nanostructured metal surface.[31−34] The transition from fluorescence enhancement to quenching is the result of a change in the relative magnitudes of the radiative and nonradiative decay rates of the fluorophore, which is a strong function of the proximity of the fluorophore to the surface of metallic NPs.[35,36]

In 2003, we reported an arrayable and highly effective label-free (or "self-labeled") method for DNA detection in which fluorescently tagged DNA hairpin probes are immobilized on a planar metal surface *via* a terminal thiol.[37] In the absence of target DNA, the immobilized hairpin DNA probe places the fluorophore in close proximity to the metal surface, quenching fluorescence *via* metal−fluorophore energy transfer.[28,38] Hybridization of target DNA to the immobilized probe moves the fluorophore out of range for quenching, leading to fluorescence as a positive signal for the DNA target. In subsequent efforts, we have demonstrated that this method provides

*Address correspondence to Benjamin_Miller@urmc.rochester.edu.

Received for review February 4, 2009 and accepted June 30, 2009.

Published online July 8, 2009.
10.1021/nn900112e CCC: $40.75

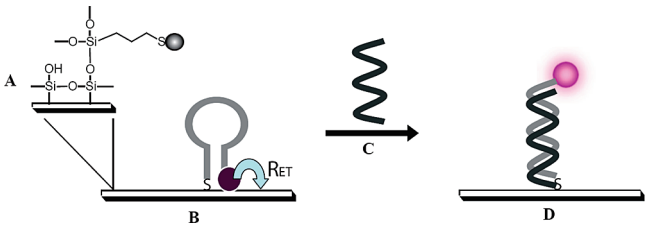

Figure 1. Working principle of the DNA detection system. (A) Ag NP attachment chemistry. The Ag NP is attached onto an MPTS-treated glass slide. (B) A fluorophore labeled DNA hairpin probe is immobilized onto the nanostructured Ag substrate *via* a terminal thiol. The hairpin structure is formed by the hybridization between the complementary nucleotides at the two ends of the DNA probe. Fluorescence from the labeled fluorophore is quenched due to energy transfer to the Ag surface (R_{ET}: rate of energy transfer). (C) Introduction of an unlabeled DNA target, of complementary sequence to the DNA probe. (D) Hybridization between the DNA probe and target moves the labeled fluorophore away from the metal surface and restores fluorescence.

exceptional sensitivity for single-base mismatches[39] and potentially allows single-spot/multicolor detection.[40] Furthermore, we have developed a general methodology for discovering hairpin probes suitable for use in this system with complete complementarity for the DNA target.[41]

In any biosensor system target sensitivity is critical, and one common strategy to enhance the target sensitivity is through signal amplification.[42] This article describes initial experiments designed to test the utility of Ag NPs as signal amplifiers in a "self-labeled" DNA detection system. A particular focus is placed on the fluorescence enhancement level as a function of the substrate surface topography (*e.g.*, NP size, substrate surface roughness, and surface coverage) and distance between the fluorophore and the substrate surface.

As in the planar Au analogue of these chips, DNA hairpin probes were first immobilized onto the Ag NP coated chips *via* the terminal thiol group (Figure 1B). Hairpin formation brings the fluorophore close to the metal, and the fluorescence is quenched due to nonradiative energy transfer to the Ag surface.[43] The addition of label-free target DNA (Figure 1C) forces the hairpin DNA to open, brings the fluorophore away from the metal surface, and subsequently restores the fluorescence (Figure 1D). Fluorescence images are acquired both before (Figure 1B) and after probe-target hybridization (Figure 1D), and the intensity change from pre- to post-hybridization serves as the signal for the presence of a specific DNA sequence that is being detected.

RESULTS AND DISCUSSION

Fabrication of the nanostructured Ag substrates was accomplished by covalently attaching Ag NPs onto 3-mercaptopropyl-trimethoxysilane (MPTS, Gelest, Inc.) treated glass chips *via* Ag^+ ion reduction from a 10 mM $AgNO_3$ solution in *N-N*-dimethylformamide (DMF, Mallinckrodt)[22,44] (Figure 1A). To examine the effect of Ag NP size and surface coverage on the detection performance, we varied the Ag exposure times from 10 min to 18 h (10 min, 20 min, 30 min, 1 h, 2 h, 3 h, 4 h, 8 h, and 18 h). A variation in Ag exposure time was anticipated to modulate the NP size and size distribution as suggested by Pastoriza-Santos *et al.*[39] After Ag substrates were fabricated, they were stored at room temperature for 2 days prior to DNA hybridization experiments, in order to minimize differences in chip-to-chip performance due to subtle variation in Ag surface oxidation.

Visual inspection of the Ag substrates fabricated under different Ag exposure times (Figure 2, left) indicates that low Ag exposure substrates (10 min, 20 min, 30 min, and 1 h) were essentially indistinguishable from bare glass, while higher Ag exposure substrates (2, 3, 4, 8, and 18 h) developed a yellow to yellow-black tinted appearance. As discussed below, we found that the low Ag exposure substrates had sufficient Ag NPs to support DNA detection.

A more quantitative characterization of the substrates was obtained by measuring the extinction spec-

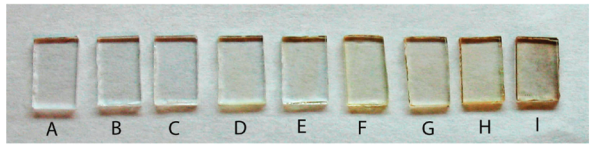

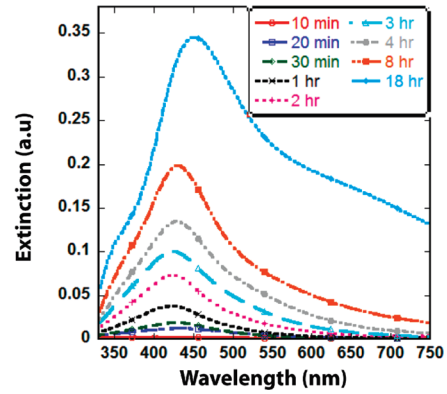

Figure 2. (Left) Image of the Ag NP substrates fabricated under different Ag exposure times: (A) 10 min, (B) 20 min, (C) 30 min, (D) 1 h, (E) 2 h, (F) 3 h, (G) 4 h, (H) 8 h, and (I) 18 h. Low Ag exposure substrates (A−D) were essentially indistinguishable from bare glass, whereas higher Ag exposure substrates developed a yellow (E−G) to yellow-black (H,I) tinted appearance. (Right) Extinction spectra of Ag substrates prepared with different Ag exposure times (10 min, 20 min, 30 min, 1 h, 2 h, 3 h, 4 h, 8 h, and 18 h). The spectra show a characteristic peak positioned at ~420 nm (substrates prepared with ≥20 min Ag exposure time). As the Ag exposure time increased from 20 min to 18 h, there was an increase in extinction magnitude associated with a red shift.

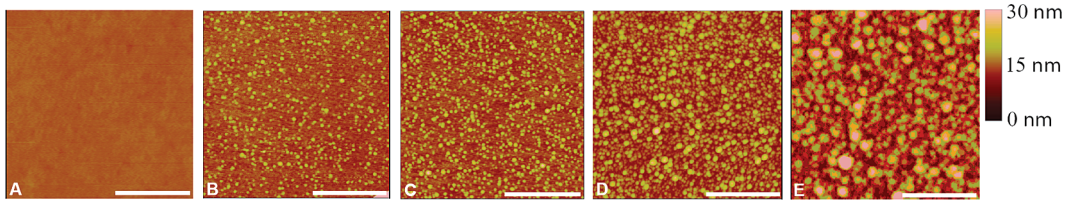

Figure 3. AFM images showing topographic features of the nanostructured Ag substrates prepared in a 10 mM $AgNO_3$ solution with different Ag exposure times: (B) 10 min, (C) 20 min, (D) 8 h, and (E) 18 h. (A) Bare glass slide only, with no Ag NP deposition. Scale bar: 400 nm. An increase in Ag exposure time was associated with an increase in the level of NP coverage and the range of NP size.

tra (Figure 2, right). Substrates prepared with Ag exposure time ≥20 min have spectra featuring a characteristic extinction peak centered at ~420 nm. At increasing Ag exposure time, this extinction peak redshifts from ~420 to 450 nm, indicating larger Ag particle formation. As one would expect, the extinction magnitude also increased with increasing Ag exposure time as a result of an increase in the amount of Ag NPs that were deposited on the substrate. Additionally, the spectra from substrates prepared with 8 and 18 h Ag exposure times developed secondary peaks positioned at ~350 nm (18 h), 400 nm (8 h), and 650 nm (18 h), respectively, suggesting that the NPs and NP aggregates formed at these higher Ag exposure times are heterogeneous (wider particle size and shape range).

To obtain a more detailed understanding of the nanostructured Ag surfaces and a better understanding of the extinction spectra, we examined the surface topography by atomic force microscopy (AFM). As shown in Figure 3, the bare glass slide (Figure 3A) demonstrates a flat surface (mean roughness = 0.58 nm as calculated by AFM), while Ag nanostructured substrates (Figure 3B−E) are characterized with mean roughness values ranging from 0.842 nm (Figure 3B) to 3.8 nm (Figure 3E). These data also clearly show that particle population density and size range are substantially influenced by Ag exposure time. For instance, a 10 min exposure time resulted in an apparent particle diameter range from 3.6 to 10 nm. This is in stark contrast to the 8 and 18 h Ag exposed substrates, where a higher level of NP coverage and wider range of apparent NP diameters (~9 to 50 nm) were observed. We hypothesize that the particles with larger apparent diameters are aggregates consisting of primary particles. The highly heterogeneous particle size distribution including the formation of NP aggregates seen on the substrate surface at higher Ag exposure time (e.g 8 and 18 h) is likely the cause for the appearance of the secondary extinction peaks at higher Ag incubation time.

Next, we set out to examine the ability of the nanostructured Ag substrates to function in the DNA detection system. Initial experiments employed a previously described DNA probe[45] (5′- TCG TTA GTG TTA GGA AAA AAT CAA ACA CTC GCG A -3′), purchased from Integrated DNA Technologies, Inc. (IDT); this probe bears a 3′- tetramethyl rhodamine (TMR) fluorophore (Ab_{max}, 559 nm; Em_{max}, 583 nm), and a 5′-thiol (disulfide form). To directly compare the detection performance of planar Au films *versus* nanostructured Ag substrates, Au films and Ag substrates were first immersed in a probe solution containing 300 nM of DNA probe and 300 nM mercaptopropanol in buffered saline. Mercaptopropanol serves as a surface blocking agent which modulates the surface density of DNA probes.[39] DNA probe-target hybridization was permitted by soaking the probe-immobilized substrates in a 2.5 μM target solution for 19 h. Fluorescence images of the TMR-DNA conjugated Ag substrates demonstrate a uniform fluorescence signal across the substrate surface, and the intensity increased from baseline (quenched) values of ~3500 to ~50000 counts posthybridization. To gain a more quantitative understanding of the intensity change from pre- to posthybridization, we also calculated the relative intensity change (*R*-value) as described by eq 1.

$$R\text{-value} = [(I_{post} - I_{blank})/(I_{pre} - I_{blank})] \quad (1)$$

where I_{post} and I_{pre} represent the post- and prehybridization intensity, and I_{blank} represents the intensity measured with unfunctionalized Ag substrates in buffered saline.

Table 1 shows different detection responses (I_{post}, I_{blank}, I_{pre}, and *R*-value) from either a planar Au film or a nanostructured Ag substrate as the sensing substrate in the DNA hybridization study. A comparison of the measured intensities between two different substrates shows that the nanostructured Ag substrate offered a dramatic (~10-fold) fluorescence enhancement over the planar Au substrate. However, it could be argued that the intensity enhancement was due to an increase in surface area from the nanostructured surface, which

TABLE 1. Comparative Detection Responses for Planar Au Film and Nanostructured Ag Substrate (20 min Ag Exposure Time) Sensors[a]

	planar Au substrate	nanostructured Ag substrate
I_{pre} (counts)	8119	38710
I_{post} (counts)	30439	517220
I_{blank} (counts)	673	2150
R-value	4	14

[a]Hybridization was performed by treating the DNA probe-immobilized substrates in a 2.5 μM target concentration for 19 h. Data are corrected for CCD integration time (10 s for planar Au, 1 s for nanostructured Ag).

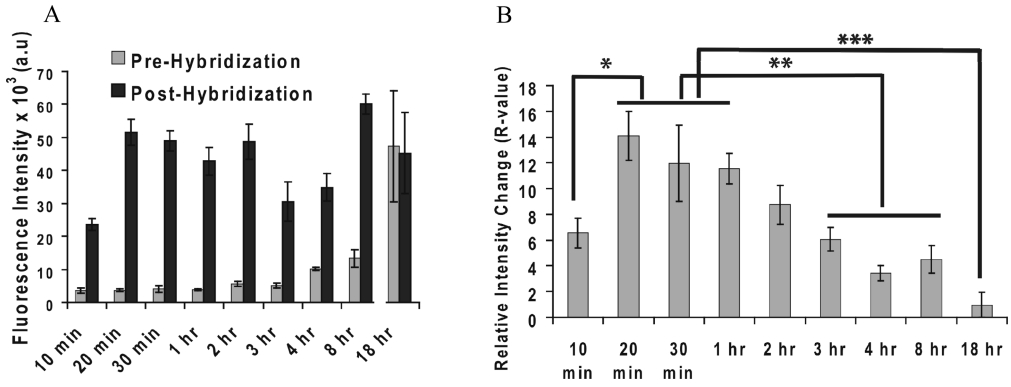

Figure 4. (A) Fluorescence intensity profile of pre- (gray) and post- (black) probe-target hybridization state as a function of substrate exposure time to Ag. Substrates were prepared in a 10 mM $AgNO_3$ solution with Ag incubation times of 10 min, 20 min, 30 min, 1 h, 2 h, 3 h, 4 h, 8 h, and 18 h. Error bars represent standard deviation. $N = 4$ (2 substrates × 2 spots/substrate). CCD integration time: 1 s. (except 18 h group, where the exposure time is 500 ms) Data are presented as means ± standard deviation. (B) Calculated *R*-value as a function of substrate exposure time to Ag (10 min, 20 min, 30 min, 1 h, 2 h, 3 h, 4 h, 8 h, and 18 h). Data are presented as means ± standard deviation, $N = 4$ (2 substrates × 2 spots/substrate). Statistical analysis was performed using one-way ANOVA with *tukey post hoc* test, Matlab. The horizontal lines above individual groups indicate there is no significant difference among each group: (*) significantly different from 10 min group; (**) significantly different from groups 3, 4, and 8 h, (***); significantly different from 18 h group (in comparison with 20 min, 30 min, and 1 h groups), $P < 0.05$.

increased the number of DNA-bounded fluorophores that are attached onto the substrate surface. To answer this question, we calculated the surface area of the nanostructured Ag substrate (20 min Ag exposure time) that was available for DNA attachment. The apparent diameter of the Ag NPs prepared with 20 min of Ag exposure time spanned from 10 to 25 nm, with a mean of 15 nm. Using an average particle density of 589 particles/μm^2 (measured by AFM) and assuming spherical particles, we arrived at an average surface area of 0.42 μm^2 per 1 μm^2 of glass. This corresponds to ~42% of the surface area available on a planar Au substrate, and neglects the fact that the available surface area is even less, given that part of each particle is in contact with the glass surface. Since the surface area available for hairpin attachment onto the Ag substrates was less than 50% of the surface area available from the planar Au substrates and the fluorescence intensity is ~10-fold higher than the fluorescence intensity acquired with the use of planar Au substrates, this suggests that the signal enhancement that was observed on the nanostructured Ag substrates was induced by the Ag NPs. However, it is important to note that although the posthybridization intensity is a dramatic 10-fold increment with the use of nanostructured Ag substrates, the *R*-value is only 3 times higher than that obtained with a planar Au film. The lower increment seen in the *R*-value is primarily due to the higher background signal obtained from nanostructured Ag substrates (where "background" in this case refers to the chip postapplication of probe, preapplication of target). A higher background signal directly decreases the signal to background ratio, and hence the *R*-value. As one can see from Table 1, I_{pre} from the nanostructured Ag substrate is approximately 4 times higher than I_{pre} from the planar Au substrate. The higher background signals can be primarily attributed to the continuum background emission of Ag rough surfaces, a commonly observed phenomenon in surface enhanced Raman scattering (SERS).[46−48] The mechanism for continuum background is conjectured to be a result of plasmon dephasing or electron tunneling.[48]

We next examined the effect of surface roughness and NP surface coverage on the detection performance by testing DNA hybridization response on substrates prepared with different Ag exposure times. We observed a dramatic increase in *R*-value (from ~6.7-fold to 14-fold; Figure 4) as the Ag exposure time employed in substrate preparation increased from 10 to 20 min. The lower *R*-value obtained from the 10 min exposure group was due mainly to the low posthybridization intensity (Figure 4A; note the similar prehybridization signal between 10 and 20 min group, as opposed to a dramatic increase in the posthybridization signal from 10 to 20 min), which suggests that the 10 min Ag substrate did not provide an adequate Ag surface area for attachment of the hairpin DNA probes. Notably, the *R*-value dropped dramatically from ~14-fold to 4.5-fold (statistically significant) as the exposure time increased from 20 min to 8 h. Substrates prepared with an 18 h Ag exposure resulted in an *R*-value as low as 1 (no difference between "pre" and "post" application of DNA target; Figure 4A).

The decrease in *R*-value obtained from substrates prepared with longer (≥3 h) Ag exposure time results primarily from decreased quenching (*e.g.*, higher signal pretarget application as shown in Figure 4A). Although this result seems counterintuitive (one might expect that the performance of the substrate would increase as the available surface area increases), we hypothesize that steric crowding of DNA probes that can occur as the NP coverage increases allows probes to interact with each other if the local density is high. This could

then restrain hairpin formation, placing the fluorophore too far away from the Ag surface for efficient quenching.[49,50] At the same time, densely packed DNA probes can also hinder the hybridization process by obstructing the accessibility of the DNA probes from the target DNA. A relatively low Ag exposure time directly lowered both the amount and the size of the Ag NPs that were deposited onto the substrate surface (Figure 3), providing more space between hairpin probes immobilized on the surface, thus alleviating this problem. To test this hypothesis, we treated nanostructured Ag substrates prepared with 18 h Ag exposure time with a probe solutions containing either 1:1 mercaptopropanol/DNA probe or 40:1 mercaptopropanol/DNA probe. Supporting our hypothesis, the substrate prepared with 1:1 mercaptopropanol/DNA probe was essentially inactive (*R*-value = 1) (Figure 4A), while increasing the mercaptopropanol/DNA probe ratio to 40:1 rescued performance (*R*-value = 30.5, data not shown). We conjecture that addition of an excess amount of mercaptopropanol lowered the amount of DNA probes immobilized on the surface, and therefore created more space between the neighboring DNA hairpin probes. A more loose packing of DNA hairpin probes on the surface prevents the neighboring DNA probes from interfering with one another, hence forming appropriate hairpin structure that enables the fluorophores to reside in the quenching sites on the substrate surface. While the observed *R*-value of 30.5 might lead one to conclude that the "rescued" 18-h substrate provided the most ideal performance characteristics, we note that the signal strength across this substrate was highly nonuniform (potentially as a result of the observed surface heterogeneity, as discussed above). Coupled with the longer Ag deposition requirement, this led us to focus on substrates prepared at shorter time points for the remainder of our studies.

While the above experiment demonstrated the importance of mercaptopropanol as a surface blocking agent to mitigate the steric crowding effect in substrates prepared with long Ag exposure time (high surface area), further work was needed to determine whether this was also true for lower density substrates. In particular, studies conducted in our group previously on planar Au chips indicated an absolute requirement for mercaptopropanol as a spacer.[39] To determine if the finding still holds in the nanostructured Ag substrate system, we examined the effect of mercaptopropanol concentration on detection performance from substrates with low Ag exposure (Figure 5). In this experiment, we varied the ratio of [MP]/[DNA] in self-assembly solutions from 0 to 25, where [DNA] represents probe DNA concentration, which was held constant at 300 nM. In the previous study, lowering the ratio of [MP] to [DNA] from 1 with the use of planar Au chips resulted in poor performance because of high background signals. In contrast, increasing the [MP]/[DNA] ratio beyond 0.2 decreased the *R*-value for nanostructured Ag substrates. These results suggest that there is no mercaptopropanol requirement when using a low Ag exposure substrate (1 h). As shown in Figure 5, both pre- and post-target intensity decreased as we increased the mercaptopropanol concentration, indicating a lower amount of DNA was being deposited on the substrate as we increased the mercaptopropanol concentration.

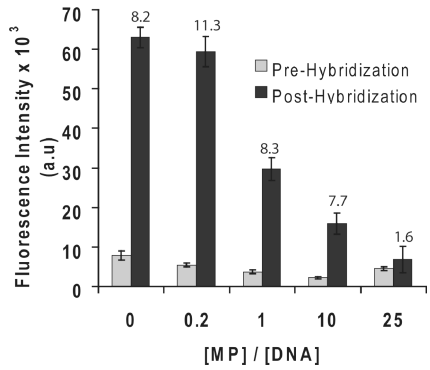

Figure 5. Fluorescence intensity profile from pre- (gray) and post- (black) probe-target hybridization examined on 1 h Ag exposure substrates as a function of [MP] to [DNA] ratio. Probe [DNA] was held constant at 300 nM for all experiments. Number placed on top of each bar represents the corresponding *R*-value. Data are presented as means ± standard deviation, *N* = 9 (3 spots/substrate × 3 substrates). CCD integration time: 1 s.

Two primary explanations may be considered with regard to this observation. First, a low particle deposition density may improve performance simply because of the physical separation of Ag NPs on the glass surface, thereby reducing the potential for interactions between hairpins on neighboring particles. Alternatively (or additionally), Mirkin and colleagues have observed a strong correlation between the radius (or curvature) of spherical Au NPs and both the loading density of and deflection angle between oligonucleotides.[51,52] While decreasing particle size led to an increase in oligonucleotide density, it also increased the deflection angle. Although both our particle and DNA systems are considerably different, it is possible that we observe a similar effect. This would suggest that deflection angle is a particularly important parameter. Efforts are underway to explore both of these possibilities in greater detail.

We also have considered the potential contribution of particle−particle junctions, or "hot spots", to the decreased quenching ability of the substrates prepared with longer deposition time. The ability of NP junctions to enhance SERS[46,47] and fluorescence[53,54] is well-known. However, enhancement occurs only when the fluorophore is sandwiched where the local high electric field is extremely high, directly between interacting particles; otherwise, the signal is quenched. As precise control of fluorophore placement is required, it seems improbable that a sufficient number of such interactions would occur such that the quenching ability seen in the

TABLE 2. Probe (P) and Target (T) Sequences with the Pathogen Sources and Minimum/Maximum Distance between the Fluorophore and the Ag NP Surface[a]

name	sequence	source	length (nm) min	length (nm) max
18mer (P)	5′-(-C6Thiol) GTT CCG TCT TGT CGG AAC (-3′ Amino C7) (TMR)-3′	E. *Coli* K 12 gene	5.4	6.9
25mer (P)	5′-(-C6Thiol) CGG ATC TCG ATG AGC TGC AGA TCC G (-3′ Amino C7) (TMR)-3′	E. *Coli* K 12 gene	7.8	9.3
30mer (P)	5′-(-C6Thiol) AGC ATA GGG ACC GTG CAG AAT CCG TAT GCT (-3′ Amino C7) (TMR)-3′	E. *Coli* TIR gene	9.5	11.0
34mer (P)	5′-(-C6Thiol) TCG TTA GTG TTA GGA AAA AAT CAA ACA CTC GCG A (-3′ Amino C7) (TMR)-3′	B. *Anthracis* pag gene	10.8	12.3
38mer (P)	5′-(-C6Thiol) AAA TTT CTT TCC CAT GAT GAG CAC CTT TAA AGA AAT TT (-3′ Amino C7) (TMR)-3′	K. *Pneumoniae* blaSHV gene	12.2	13.7
47mer (P)	5′-(-C6Thiol) CGC TCT GGA AAT GTT CAA TGA GGA CTA TGT GAC ATT CCC CAG GGA CG (-3′ Amino C7) (TMR)-3′	E. *Coli* plasmid pARS3 gene	15.2	16.7
18mer (T)	5′-GTT CCG ACA AGA CGG AAC-3′			
25mer (T)	5′-CGG ATC TGC AGC TCA TCG AGA TCC G-3′			
30mer (T)	5′ -AGC ATA CGG ATT CTG CAC GGT CCC TAT GCT-3′			
34mer (T)	5′ -TCG CGA GTG TTT GAT TTT TTC CTA ACA CTA ACG A-3′			
38mer (T)	5′ -AAA TTT CTT TAA AGG TGC TCA TCA TGG GAA AGA AAT TT-3′			
47mer (T)	5′-CGT CCC TGG GGA ATG TCA CAT AGT CCT CAT TGA ACA TTT CCA GAG CG-3′			

[a]Underlined sequences represent the nontarget specific sequences that were incorporated at both termini of the oligonucleotides for hairpin formation. The minimum distance was calculated assuming the fluorophore was folded towards the backbone of the DNA, and the maximum distance was calculated assuming the fluorophore was folded away from the backbone.

18-h substrate is significantly reduced. However, we cannot rule this out *a priori*.

While limit of detection (LOD) measurements on sensors at an early stage of development are problematic at best, they nevertheless provide a benchmark for future optimization. To examine the LOD in this case, we applied target solutions with various concentrations (2.5 μM, 1 μM, 100 nM, 10 nM, 100 pM, 10 pM, and 0 pM) to the substrate prepared with a 1 h Ag exposure time and incorporating a [MP]/[DNA] ratio of 0.2. For this unoptimized system, LOD was found to be 100 pM (Supporting Information), which is comparable with other label-free optical DNA detection systems.[4] We anticipate that this can be substantially improved. Several methods that can potentially reduce LOD will be investigated, including the employment of fluidic components and manipulation of overlap between the NP extinction spectra and the excitation/emission wavelength of the fluorophores, as well as adjusting the relative ratio of [MP] and [DNA] in the system.

Fluorescence enhancement induced by metallic NPs is a result of the interaction between the excited-state fluorophore and an enhanced electric field surrounding the metallic NPs, which is induced by the incident light. Several groups have reported experimental results indicating that the level of fluorescence enhancement is strongly distance-dependent.[33,34,55,56] Others have also shown that the magnitude of the surrounding electric field varies at different locations relative to particle surface, based on different theoretical calculations including finite-difference time-domain (FDTD),[53,57] multiple multipole method,[58] and quasistatic approximation.[59] For most of the aforementioned simulations, the magnitude of the surrounding electric field is found to be inversely proportional to the distance away from the surface of the metallic NPs. However, quenching usually takes place at very close proximity to the particle surface (<5 nm).[23,60] As a result, one would expect to locate a position away from the surface of metallic NPs at which an optimal fluorescence enhancement would be observed and where enhancement will dominate over quenching.

In our system, we can easily adjust the distance between the fluorophore and the surface of Ag NPs, by varying the number of nucleotides in the DNA hairpin probe and in the cDNA target. The distance between the fluorophore and the Ag surface can then be calculated by multiplying the number of nucleotides by 3.4 Å (the rise per base pair), given that the persistence length of the duplex DNA is ~50 nm in solution.[61−63] Therefore, we designed hairpin probes with different numbers of nucleotides ranging from 18mer to 47mer (Table 2), providing a distance range of 5.4 to 16.7 nm. The sequence, pathogen source, and corresponding minimum and maximum distance between the fluorophore and the Ag surface that were used for the length study are given in Table 2. The minimum and maximum distance between the fluorophore and the Ag surface were calculated assuming free rotation of the fluorophore, where the fluorophore can potentially fold toward (|duplex length| − |*C*6|, min) or away (|duplex length| + |*C*6|, max) from the backbone of the DNA (distance rise per base pair, 0.34 nm;[63] C−C bond length, 1.5 Å[64]).

Probe sequences were obtained from National Center for Biotechnology Information (NCBI) database[65] and were analyzed for suitability as hairpin probes using our previously described methodology.[41] All DNA probes for this study were purchased from Midland Certified Reagent Company (Midland), bearing a 3′- TMR fluorophore (Ab_{max}, 543 nm; Em_{max}, 571 nm) and a 5′trityl- thiol, and it was left in the protected form through out the experiment. All DNA targets were purchased from IDT.

Ag substrates used here were prepared in a 10 mM $AgNO_3$ solution for 1 h, and subsequently incubated in a probe solution consisting of 60 nM of mercaptopropanol

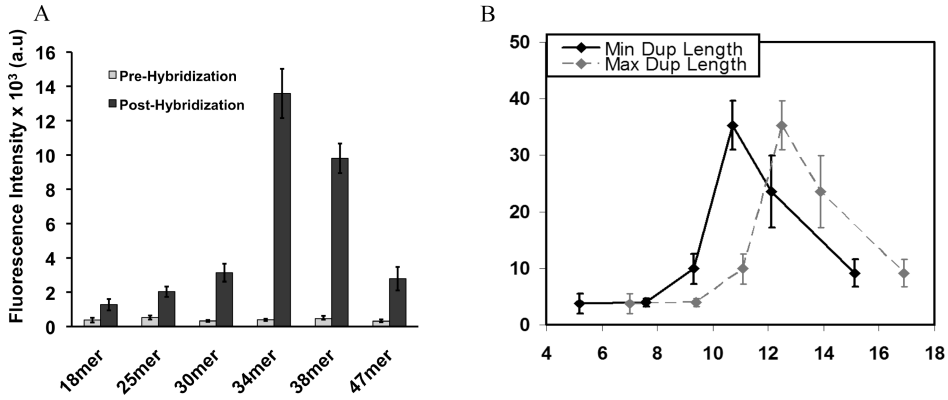

Figure 6. (A) Pre- (gray) and post- (black) probe-target hybridization fluorescence intensity profile of TMR−DNA on the nanostructured Ag substrates prepared in a 10 mM $AgNO_3$ solution for 1 h with different DNA probes (18mer, 25mer, 30mer, 34mer, 38mer, and 47mer). $N = 9$ (3 substrates × 3 spots/substrate). CCD exposure time: 500 ms. (B) Calculated relative intensity change (R-value) as a function of the distance between the fluorophore and the substrate surface. $N = 9$ (3 substrates × 3 spots/substrate). The solid and dashed lines represent the calculated minimum and maximum distance between the fluorophore and the Ag surface, respectively. Data are presented as means ± standard deviation.

and 300 nM probe DNA in buffered saline, a ratio determined to give the highest R-value for substrates prepared with this amount of Ag exposure (Figure 5). Hybridization was allowed to proceed for 19 h at room temperature, in order to ensure observed differences were not the result of differences in hybridization efficiency. Figure 6A shows the fluorescence intensity profile from pre- (gray) to post- (black) hybridization with the use of different DNA hairpin probes. Figure 6B plots the calculated R-value as a function of the corresponding distance between the fluorophore and the Ag surface. As shown in Figure 6A, the prehybridization intensities were very much alike for each probe, indicating consistent fluorescence quenching and stable hairpin formation. In contrast, the posthybridization intensity increased initially from the 18mer to the 30mer, reached a maximum enhancement level of ~35-fold intensity for the 34mer, and then decreased at farther distances relative to the nanostructured Ag surface. This finding agrees with the work conducted by Malicka et al., where a maximum fluorescence enhancement was observed at a distance approximately 90 Å from an Ag mirror surface.[55]

The novel properties of nanoscale materials present many unique opportunities for sensor development. We have demonstrated initial experiments designed to examine the utility of nanostructured Ag substrates in a "self-labeled" DNA detection system with an unoptimized limit of detection of 100 pM. As expected, the nanostructured Ag substrates provide both quenching of nonspecific fluorescence and enhancement of the signal that is produced when the fluorophore is separated from the Ag substrate. The use of nanostructured Ag substrates demonstrated a strong (~10-fold) improvement in fluorescence signal over planar Au substrates for equivalent amounts of analyte. It was found that the surface roughness of the nanostructured substrate, particle size (since the two are interrelated), and the amount of Ag that was deposited onto the surface can be varied by controlling the Ag exposure time in a constant concentration of $AgNO_3$ solution. Furthermore, detection performance and signals were strongly dependent on both the surface roughness/NP coverage and the distance between the fluorophore and the Ag substrate surface. In this study, Ag exposure time of 20 min, 30 min, and 1 h in a 10 mM $AgNO_3$ solution provided optimal detection response in a probe solution consisting of 5 parts of DNA probe to 1 part of mercaptopropanol. Substrates prepared with higher Ag exposure times resulted in lower detection responses, potentially resulting from a steric crowding effect. Consistent with theoretical predictions of a strong distance dependence on metal particle-mediated fluorescence enhancement, we observed that DNA hairpin probe containing 34 nucleotides gave the highest postintensity and highest R-value with the use of nanostructured Ag substrate prepared with a 1 h Ag exposure time. These findings collectively demonstrate the significant role of nanostructured substrate surface topography, local probe density, and probe length selection for a DNA detection system utilizing metallic NPs as the sensing substrate. Of further interest is the fact that the low-exposure Ag substrates are transparent, which potentially allows for their incorporation into novel instrument designs, such as flow-through devices in which imaging occurs from the opposite face from the functionalized Ag.

EXPERIMENTAL METHODS

Fabrication of Substrates. First, a standard 75 × 25-mm glass microscope slide was broken into ~5 × 10-mm chips. Next, the glass chips were cleaned by soaking them in a piranha solution (H_2SO_4:35% H_2O_2; 3:1) for 15 min (CAUTION, piranha solution is highly caustic and can react explosively with organic materials). The glass chips were then rinsed with distilled, deionized (DDI) water, soaked in a 10 M NaOH solution for 5 min, rinsed again with DDI water, and finally dried under nitrogen gas. The cleaned glass chips were silanized by incubating in a solution com-

posed of 1% 3-mercaptopropyl trimethoxysilane (MPTS), 95% methanol, and 4% 1 mM acetic acid at room temperature for 30 min. The silanized glass chips were then sonicated (300-W Vibracell probe sonicator, Sonic & Material Inc.) in a 95% ethanol:5% water solution for 2 min, and dried under nitrogen gas. Coating of the silanized glass chips with Ag NPs was accomplished by incubating them in a solution of 10 mM $AgNO_3$ in DMF at room temperature. Ag^+ ion was reduced by DMF as first proposed by the Liz-Marzan group.[44] The chips were washed after Ag exposure by sonication in a 95% ethanol:5% water solution for 4 min, dried under nitrogen gas, and stored at room temperature for 2 days prior to DNA attachment There is a slight but noticeable batch-to-batch variation among the Ag substrates (based on the prehybridization responses, I_{pre}) since factors such as temperature and solvent hydration can affect the kinetics of particle formation. To eliminate this potential variation, every experiment was carried out using substrates prepared within the same batch. Results showed that there is little variation among substrates prepared under one batch. Planar Au films were fabricated based on the protocol described in Strohsahl *et al.*[45]

Self-Assembly. Self-assembly of DNA hairpin probes on metal substrates was accomplished by incubating each substrate in a solution consisting of 300 nM probe DNA and different concentrations of mercaptopropanol in buffered saline (500 mM NaCl, 20 mM cacodylic acid, and 0.5 mM ethylenediaminetetraacetic acid (EDTA), pH = 7.0) at room temperature for 2 h. Next, nonspecifically bound DNA probes were removed by washing the substrates with boiling DDI water for 30 s. Substrates were then air-dried and kept in the dark at room temperature for 45 min. Hairpin formation was promoted by adding buffered saline to the dried substrates, then soaking them in the dark at room temperature for 45 min. Prehybridization fluorescence measurements were made for each substrate after removal from the saline solution. Finally, the Ag substrates were immersed in a 2.5 μM label-free DNA target solution overnight followed by imaging of the TMR-DNA functionalized substrates as described in the following section.

Imaging. Fluorescence measurements were performed using an Olympus BX-60 fluorescence microscope equipped with a thermoelectrically (TE) cooled charge coupled device (CCD). Samples were excited with incident light from a Hg lamp (100-W), which was filtered with an excitation bandpass filter (531 ± 20 nm), reflected by a dichroic mirror, and guided through a 10× objective lens. The emitted light was collected by the CCD after being directed from the sample, through the objective, the dichroic mirror, and a bandpass filter (593 ± 20 nm). Fluorescence images were analyzed using Image J software.[66]

Characterization of Substrates. Extinction spectra of Ag substrates were measured by Perkin-Elmer Lambda 950 UV−vis, with a wavelength range spanning 330 to 750 nm. All measurements were corrected by the background signal generated by glass slide alone. AFM images of the Ag substrates were obtained using a Digital Instruments Nanoscope IIIa operated in tapping mode using a Si tip (300 kHz, 40 N/m). NP height measurements were made offline using Digital Instrument (DI) software.

Acknowledgment. The authors gratefully acknowledge the New York State Foundation for Science, Technology, and Innovation (NYSTAR), and the Department of Energy Office of Basic Energy Sciences for financial support.

Supporting Information Available: Limit of detection (LOD) measurement. This material is available free of charge *via* the Internet at http://pubs.acs.org.

REFERENCES AND NOTES

1. Harrington, C. A.; Rosenow, C.; Retief, J. Monitoring Gene Expression Using DNA Microarrays. *Curr. Opin. Microbiol.* **2000**, *3*, 285–291.
2. Lockhart, D. J.; Winzeler, E. A. Genomics, Gene Expression and DNA Arrays. *Nature* **2000**, *405*, 827–836.
3. Heller, M. J. DNA Microarray Technology: Devices, Systems, and Applications. *Annu. Rev. Biomed. Eng.* **2002**, *4*, 129–153.
4. Sassolas, A.; Leca-Bouvier, B. D.; Blum, L. DNA Biosensors and Microarrays. *J. Chem. Rev.* **2008**, *108*, 109–139.
5. Tyagi, S.; Kramer, F. R. Molecular Beacon: Probe that Fluoresce upon Hybridization. *Nat. Biotechnol.* **1996**, *14*, 303–308.
6. Dubertret, B.; Calame, M.; Libchaber, A. J. Single-Mismatch Detection Using Gold-Quenched Fluorescent Oligonucleotides. *Nat. Biotechnol.* **2001**, *19*, 365–370.
7. Steemers, F. J.; Ferguson, J. A.; Walt, D. R. Screening Unlabeled DNA Targets with Randomly Ordered Fiber-Optic Gene Arrays. *Nat. Biotechnol.* **2000**, *18*, 91–94.
8. Tsourkas, A.; Behlke, M. A.; Bao, G. Structure-Function Relationships of Shared-Stem and Conventional Molecular Beacon. *Nucleic Acids Res.* **2002**, *30*, 4208–4215.
9. Fang, X. H.; Liu, X. J.; Schuster, S.; Tan, W. H. Designing a Novel Molecular Beacon for Surface-Immobilized DNA Hybridization Studies. *J. Am. Chem. Soc.* **1999**, *121*, 2921–2922.
10. Wang, K.; Tang, Z.; Yang, C. J.; Kim, Y.; Fang, X.; Li, W.; Wu, Y.; Medley, C. D.; Cao, Z.; Colon, P.; Lin, H.; Tan, W. Molecular Engineering of DNA: Molecular Beacons. *Angew. Chem., Int. Ed.* **2008**, *47*, 2–17.
11. Fan, C. H.; Plaxco, K. W.; Heeger, A. J. Electrochemical Interrogation of Conformational Changes as a Reagentless Method for the Sequence-Specific Detection of DNA. *Proc. Natl. Acad. Sci. U.S.A.* **2003**, *100*, 9134–9137.
12. Pan, S. L.; Rothberg, L. Chemical Control of Electrode Functionalization for Detection of DNA Hybridization by Electrochemical Impedance Spectroscopy. *Langmuir* **2005**, *21*, 1022–1027.
13. Drummond, T. G.; Hill, M. G.; Barton, J. K. Electrochemical DNA Biosensor. *Nat. Biotechnol.* **2003**, *21*, 1192–1199.
14. Erdem, A.; Pividori, M. I.; Lermo, A.; Bonanni, A.; del Valle, M.; Alegret, S. Genomagnetic Assay Based on Label-Free Electrochemical Detection Using Magneto-Composite Electrodes. *Sens. Actuators, B* **2006**, *114*, 591–598.
15. Mannelli, F.; Minunni, A.; Tombelli, S.; Wang, R. H.; Spiriti, M. M.; Mascini, M. Direct Immobilisation of DNA Probes for the Development of Affinity Biosensors. *Bioelectrochemistry* **2005**, *66*, 129–138.
16. Yao, X.; Li, X.; Toledo, F.; Zurita-Lopez, C.; Gutova, M.; Momand, J.; Zhou, F. M. Sub-Attomole Oligonucleotide and p53 cDNA Determinations *via* a High-Resolution Surface Plasmon Resonance Combined with Oligonucleotides-Capped Gold Nanoparticle Signal Amplification. *Anal. Biochem.* **2006**, *354*, 220–228.
17. Janshoff, A.; Galla, H. J.; Steinem, C. Piezoelectric Mass-Sensing Devices as Biosensors-An Alternative to Optical Biosensors. *Angew. Chem., Int. Ed.* **2000**, *39*, 4004–4032.
18. Su, X. D.; Wu, Y. J.; Knoll, W. Comparison of Surface Plasmon Resonance Spectroscopy and Quartz Crystal Microbalance Techniques for studying DNA Assembly and Hybridization. *Biosens. Bioelectron.* **2005**, *21*, 719–726.
19. Li, H. X.; Rothberg, L. Colorimetric Detection of DNA Sequences Based on Electrostatic Interactions with Unmodified Gold Nanoparticles. *Proc. Natl. Acad. Sci. U.S.A.* **2004**, *101*, 14036–14039.
20. Storhoff, J. J.; Lucas, A. D.; Garimella, V.; Bao, Y. P.; Muller, U. R. Homogeneous Detection of Unamplified Genomic DNA Sequences Based on Colorimetric Scatter of Gold Nanoparticle Probes. *Nat. Biotechnol.* **2004**, *22*, 883–887.
21. Taton, T. A.; Mirkin, C. A.; Letsinger, R. L. Sanometric DNA Array Detection with Nanoparticle Probes. *Science* **2000**, *289*, 1757–1760.
22. Sabanayagam, C. R.; Lakowicz, J. R. Increasing the Sensitivity of DNA Microarrays by Metal-Enhanced Fluorescence Using Surface-Bound Silver Nanoparticles. *Nucleic Acids Res.* **2007**, *35*, e13.
23. Bharadwaj, P.; Anger, P.; Novotny, L. Nanoplasmonic Enhancement of Single-Molecule Fluorescence. *Nanotechnology* **2007**, *18*, 044017.
24. Thomas, M.; Greffet, J. J.; Carminati, R.; Arias-Gonzalez, J. R. Single-Molecule Spontaneous Emission Close to Absorbing Nanostructures. *Appl. Phys. Lett.* **2004**, *85*, 3863–3865.

25. Chen, Y.; Munechuka, K.; Ginger, D. S. Dependence of Fluorescence Intensity on the Spectral Overlap between Fluorophores and Plasmon Resonant Single Silver Nanoparticles. *Nano Lett.* **2007**, *7*, 690.
26. Strank, O.; Nooney, R.; McDonagh, C.; MacCraith, B. D. Optimization of Nanoparticle Size for Plasmonic Enhancement of Fluorescence. *Plasmonics* **2007**, *2*, 15–22.
27. Andreussi, O.; Corni, S.; Mennucci, B.; Tomasi, J. Radiative and Nonradiative Decay Rates of a Molecule Close to a Metal Particle of Complex Shape. *J. Chem. Phys.* **2004**, *121*, 10190–10202.
28. Lakowicz, J. R. *Principles of Fluorescence Spectroscopy,* 3rd ed.; Springer: New York, 2006.
29. Lakowicz, J. R.; Shen, Y. B.; D'Auria, S.; Malicka, J.; Fang, J. Y.; Gryczynski, Z.; Gryczynski, I. Radiative Decay Engineering 2. Effect of Silver Island Films on Fluorescence Intensity, Lifetimes, and Resonance Energy Transfer. *Anal. Biochem.* **2002**, *301*, 261–277.
30. Aslan, K.; Huang, J.; Wilson, G. M.; Geddes, C. D. Metal-Enhanced Fluorescence-Based RNA Sensing. *J. Am. Chem. Soc.* **2006**, *128*, 4206–4207.
31. Aslan, K.; Gryczynski, I.; Malicka, J.; Matveeva, E.; Lakowicz, J. R.; Geddes, C. D. Metal-Enhanced Fluorescence: An Emerging Tool in Biotechnology. *Curr. Opion. Biotechnol.* **2005**, *16*, 55–62.
32. Lakowicz, J. R. Review Radiative Decay Engineering: Biophysical and Biomedical Applications. *Anal. Biochem.* **2001**, *298*, 1–24.
33. Anger, P.; Bharadwaj, P.; Novotny, L. Enhancement and Quenching of Single-Molecule Fluorescence. *Phys. Rev. Lett.* **2006**, *96*, 113002.
34. Bharadwaj, P.; Novotny, L. Spectral Dependence of Single Molecule Fluorescence Enhancement. *Opt. Express* **2007**, *15*, 14266–14274.
35. Kuhn, S.; Hakanson, U.; Rogobete, L.; Sandoghdar, V. Enhancement of Single-Molecule Fluorescence Using a Gold Nanoparticle as an Optical Nanoantenna. *Phys. Rev. Lett.* **2006**, *97*, 17402.
36. Dulkeith, E.; Ringler, M.; Klar, T. A.; Feldmann, J.; Javier, A. M.; Parak, W. J. Gold Nanoparticles Quench Fluorescence by Phase Induced Radiative Rate Suppression. *Nano Lett.* **2005**, *5*, 585–589.
37. Du, H.; Disney, M. D.; Miller, B. L.; Krauss, T. D. Hybridization-Based Unquenching of DNA Hairpins on Au Surfaces: Prototypical "Molecular Beacon" Biosensors. *J. Am. Chem. Soc.* **2003**, *125*, 4012–4013.
38. Dulkeith, E.; Morteani, A. C.; Niedereichholz, T.; Klar, T. A.; Feldmann, J.; Levi, S. A.; van Veggel, F. C. J. M.; Reinhoudt, D. N.; Moller, M.; Gittins, D. I. Fluorescence Quenching of Dye Molecules near Gold Nanoparticles: Radiative and Nonradiative Effects. *Phys. Rev. Lett.* **2002**, *89*, 203002.
39. Du, H.; Strohsahl, C. M.; Camera, J.; Miller, B. L.; Krauss, T. D. Sensitivity and Specificity of Metal Surface-Immobilized "Molecular Beacon" Biosensors. *J. Am. Chem. Soc.* **2005**, *127*, 7932–40.
40. Strohsahl, C. M.; Du, H.; Miller, B. L.; Krauss, T. D. Towards Single-Spot Multianalyte Molecular Beacon Biosensors. *Talanta* **2005**, *67*, 479–485.
41. Strohsahl, C. M.; Krauss, T. D.; Miller, B. L. Identification of High-Stringency DNA Hairpin Probes by Partial Gene-Folding. *Biosens. Bioelectron.* **2007**, *23*, 233–40.
42. DeLouise, L. A.; Kou, P. M.; Miller, B. L. Cross-Correlation of Optical Microcavity Biosensor Response with Immobilized Enzyme Activity. Insights into Biosensors Sensitivity. *Anal. Chem.* **2005**, *77*, 3222–3230.
43. Sokolv, K.; Chumanov, G.; Cotton, T. M. Enhancement of Molecular Fluorescence near the Surface of Colloidal Metal Films. *Anal. Chem.* **1998**, *70*, 3898.
44. Pastoriza-Santos, I.; Liz-Marzan, L. M. Formation and Stabilization of Silver Nanoparticles through Reduction by *N,N*-Dimethylformamide. *Langmuir* **1999**, *15*, 948–951.
45. Strohsahl, C. M.; Miller, B. L.; Krauss, T. D. Preparation and Use of Metal Surface-Immobilized DNA Hairpins for the Detection of Oligonucleotides. *Nat. Protoc.* **2007**, *2*, 2105–2110.
46. Nie, S.; Emory, S. R. Probing Single Molecules and Single Nanoparticles by Surface-Enhanced Raman Scattering. *Science* **1997**, *275*, 1102–1106.
47. Michaels, A. M.; Jiang, n/a; Brus, L. E. Ag Nanocrystal Junctions as the Site for Surface-Enhanced Raman Scattering of Single Rhodamine 6G Molecules. *J. Phys. Chem. B* **2000**, *104*, 11965–11971.
48. Michaels, A. M.; Nirmal, M.; Brus, L. E. Surface Enhanced Raman Spectroscopy of Individual Rhodamine 6G Molecules on Large Ag Nanocrystals. *J. Am. Chem. Soc.* **1999**, *121*, 9932–9939.
49. Maxwell, D. J.; Taylor, J. R.; Nie, S. M. Self-Assembled Nanoparticle Probes for Recognition and Detection of Biomolecules. *J. Am. Chem. Soc.* **2002**, *124*, 9606–9612.
50. Zhang, J.; Song, S. P.; Zhang, L. Y.; Wang, L. H.; Wu, H. P.; Pan, D.; Fan, C. Sequence-Specific Detection of Femtomolar DNA *via* a Chronocoulometric DNA Sensor (CDS): Effects of Nanoparticle-Mediated Amplification and Nanoscale Control of DNA Assembly at Electrodes. *J. Am. Chem. Soc.* **2006**, *128*, 8575–8580.
51. Hill, H. D.; Millstone, J. E.; Banholzer, M. J.; Mirkin, C. A. The Role Radius of Curvature Plays in Thiolated Oligonucleotide Loading on Gold Nanoparticles. *ACS Nano* **2009**, *3*, 418–424.
52. Hurst, S. J.; Lytton-Jean, A. K. R.; Mirkin, C. A. Maximizing DNA Loading on a Range of Gold Nanoparticle Sizes. *Anal. Chem.* **2006**, *78*, 8313–8318.
53. Zhang, J.; Fu, Y.; Chowdhury, M. H.; Lakowicz, J. R. Metal-Enhanced Single-Molecule Fluorescence on Silver Particle Monomer and Dimer: Coupling Effect between Metal Particles. *Nano Lett.* **2007**, *7*, 2101–2107.
54. Bek, A.; Jansen, R.; Ringler, M.; Mayilo, S.; Thomas, A. K.; Feldmann, J. Fluorescence Enhancement in Hot Spots of AFM-Designed Gold Nanoparticles Sandwiches. *Nano Lett.* **2008**, *8*, 485–490.
55. Malicka, J.; Gryczynski, I.; Gryczynski, Z.; Lakowicz, J. R. Effects of Fluorophore-to-Silver Distance on the Emission of Cyanine-Dye-Labeled Oligonucleotides. *Anal. Biochem.* **2003**, *315*, 57–66.
56. Cheng, D. M.; Xu, Q. H. Separation Distance Dependent Fluorescence Enhancement of Fluorescein Isothiocyanate by Silver Nanoparticles. *Chem. Commun.* **2007**, *3*, 248–250.
57. Novotny, L.; Bian, R. X.; Xie, X. S. Theory of Nanometric Optical Tweezers. *Phys. Rev. Lett.* **1997**, *79*, 645–648.
58. Novotny, L.; Pohl, D. W.; Hecht, B. Scanning Near-Field Optical Probe with Ultrasmall Spot Size. *Opt. Lett.* **1995**, *20*, 970–972.
59. Kelly, K. L.; Coronado, E.; Zhao, L. L.; Schatz, G. C. The Optical Properties of Metal Nanoparticles: the Influence of Size, Shape, and Dielectric Environment. *J. Phy. Chem. B.* **2003**, *107*, 668–677.
60. Frey, H. G.; Witt, S.; Felderer, K.; Guckenberger, R. High Resolution Imaging of Single Fluorescent Molecules with the Optical Near-Field of a Metal Tip. *Phys. Rev. Lett.* **2004**, *93*, 200801.
61. Garcia, H. G.; Grayson, P.; Han, L.; Inamdar, M.; Kondev, J.; Nelson, P. C.; Phillips, R.; Widom, J.; Wiggins, P. A. Review Biological Consequences of Tightly Bent DNA: The Other Life of a Macromolecular Celebrity. *Biopolymers* **2007**, *85*, 115–130.
62. Gueroui, Z.; Libchaber, A. Single-Molecule Measurements of Gold-Quenched Quantum Dots. *Phys. Rev. Lett.* **2004**, *93*, 166108–166111.
63. Voet, D.; Voet, J. G. *Biochemistry,* 3rd ed.; J. Wiley & Sons: New York, 1995.
64. Lide, D. R. *CRC Handbook of Chemistry and Physics*, 86th ed.; Taylor and Francis: Boca Raton, FL, 2005; p 919..
65. Available at http://www.ncbi.nlm.nih.gov.
66. Abramoff, M. D.; Magelhaes, P. J.; Ram, S. J. Image Processing with ImageJ. *Biophoton. Int.* **2004**, *11*, 36–42.